Design and Fabrication of the Harvard Ambulatory Micro-Robot

A.T. Baisch and R.J. Wood

Abstract Here we present the design and fabrication of a 90mg hexapedal microrobot with overall footprint dimensions of 17 mm long x 23 mm wide. Utilizing smart composite microstructure fabrication techniques, we combine composite materials and polymers to form articulated structures that assemble into an eight degree of freedom robot. Using thin foil shape memory alloy actuators and inspiration from biology we demonstrate the feasibility of manufacturing a robot with insect-like morphology and gait patterns. This work is a foundational step towards the creation of an insect-scale hexapod robot which will be robust both structurally and with respect to locomotion across a wide variety of terrains.

1 Introduction

Autonomous mobile robots are a desirable alternative to sending humans into hazardous environments such as natural disasters. Such robots equipped with embedded sensors could provide quick reconnaissance regarding survivor locations and chemical toxicity levels, or simply map out an area for rescue workers. In these situations, large numbers of insect-scale devices using swarm algorithms might be more efficient than larger, less agile, and more expensive robots.

There are multiple potential locomotion modes for microrobots, including crawling [10], rolling, flying [24], jumping [3], gliding [26], slithering, or rockets [22]. This work focuses on ambulation, which has been shown to be robust and efficient on diverse terrain by studies of insect locomotion. Some species of cockroach are

Andrew T. Baisch
Harvard University School of Engineering and Applied Sciences, Cambridge, MA e-mail: abaisch@seas.harvard.edu

Robert J. Wood
Harvard University School of Engineering and Applied Sciences, Cambridge, MA e-mail: rjwood@eecs.harvard.edu

capable of running at speeds up to 20 body lengths per second (*Blaberus discoidalis*) and even 40 body lengths per second (*Periplaneta Americana*) [8]. Cockroaches are known to maintain high speed ambulation across rough, uneven terrain [21] and provide further design inspiration with their ability to climb sheer vertical and even inverted surfaces [17]. Furthermore, they have efficient navigational aids such as antennae that allow obstacle avoidance even in low lighting [13]. These aspects of insect morphology enable robust locomotion, and we strive to translate the underlying principles into designs for an insect-scale ambulatory robot.

Roboticists have already proven the importance of using nature as a design guide, as evidenced by legged robots that are more agile than their wheeled counterparts [19],[15],[16]. There has been work to create climbing robots for rough [11] or smooth [12] surfaces, and even efforts to integrate insect-like proximity sensors for navigation along walls [14], [4]. Others have attempted to use MEMS fabrication to create silicon insect-scale ambulatory robots [6], [27], [5].

Our goal is to combine many of these functions into a single autonomous millimeter-scale robot. This work focuses on the design and fabrication of thoracic and leg mechanics, actuation, and electronics required to achieve such a goal. Furthermore we examine potential modes of attachment as a preliminary study on scaling vertical surfaces with a microrobot. We conclude with an overview of remaining research topics towards the creation of a fully autonomous ambulatory robotic insect.

2 Robot Design

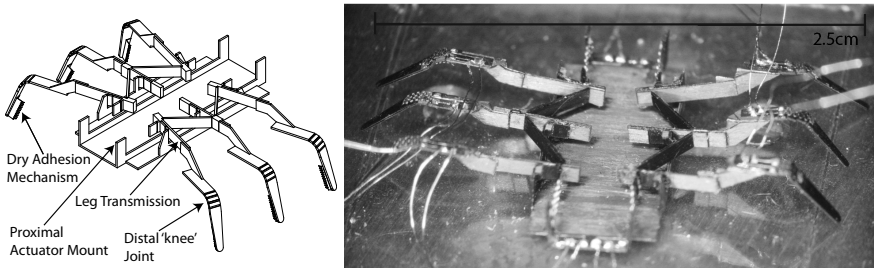

Fig. 1 Notional design of the thorax and legs of the Harvard Ambulatory Microrobot (left) and initial prototype (right)

The design of the Harvard Ambulatory Microrobot (HAMR), presented in Fig. 1, was motivated by several factors, including available fabrication techniques, and the necessary body mechanics to achieve gaits inspired by insects. Important constraints in designing a microrobot are brought about by the fabrication techniques and materials that may be used. A solution will be discussed in Section 3, however our

designs will be based on standardized components such as rigid links, flexure joints, and linear actuators.

Insect, and in particular cockroach, morphology demonstrates the utility of a hexapedal structure for static stability during locomotion. As opposed to bipedal or quadrupedal animals, hexapods typically exhibit static stability through the duration of their gait (for non-running gaits). We chose six legs as opposed to a greater number primarily for fabrication simplicity. Additionally, we believe a sprawled posture will be beneficial for future endeavors such as scaling vertical surfaces [9]. Our design adheres to insect-scale physical parameters: 100mg maximum body mass (excluding electronics), and overall footprint of approximately $2cm^2$.

To achieve maximum functionality in diverse environments HAMR must be capable of attaining and transitioning between numerous basis gaits. In forward locomotion, hexapods typically exhibit an alternating tripod gait (Fig. 2a) in which the anterior and posterior leg on one side of the body and the opposite center leg are in ground contact during each half period of a gait. The stance legs move towards the rear of the body, propelling the body center of mass (COM) forward. During the airborne, or swing phase, legs come into ground contact when stance legs reach their maximum displacement. Alternating tripod is not the sole required motion, however, since our robot must have maneuverability in diverse environments. We must achieve zero-radius turns (Fig. 2b) and/or gradual turns, which require phase adjustment between legs. As in animals, transitions between gaits must occur continually in response to locomotion speed and terrain. This dynamic gait modulation (DGM) must be achievable without unnecessarily increasing the robot complexity, power and control requirements, or exceeding physical constraints.

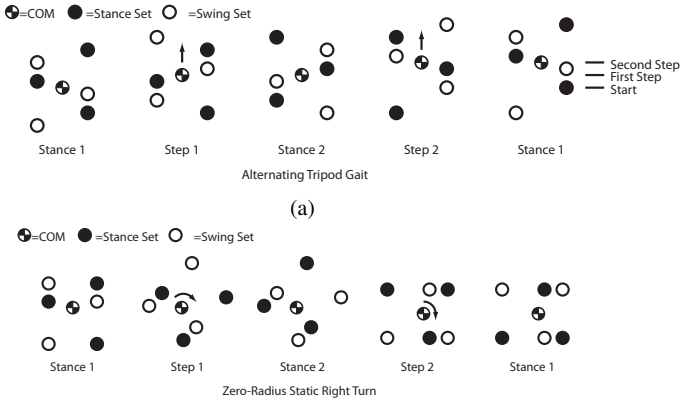

Fig. 2 Hexapods can achieve a variety of gaits. a) An alternating tripod gait propels the body COM forward during each step, as indicated by horizontal lines. b) Proposed gait pattern for zero-radius static turns that operate when one or more of HAMR's stance legs slips during rotation.

2.1 Thoracic Mechanics

To achieve the design requirements, HAMR's mechanics are separated into two distinct modes of actuation: proximal, which is controlled in the thorax, and distal, or lower-leg control. This feature allows simple control of transverse (parallel to ground) leg movement through two thoracic DOFs and gait definition by addition or removal of each of the six legs to the stance set.

HAMR's proximal mechanics consist of two leg transmissions, each controlling three legs. The transmissions are mirrored across the sagittal plane, and therefore legs are grouped on each side of the robot's thorax. An alternative grouping would couple the anterior and posterior leg with the center leg on the opposite side of the body. However, this method would require crossing linkages and dividing the single actuation plane into two. With the two leg transmissions coplanar, fabrication complexity is minimized and it ensures that the body center of mass lies in the sagittal plane. Any mass asymmetry could lead to difficulties in attaining a stable gait.

2.1.1 Kinematics

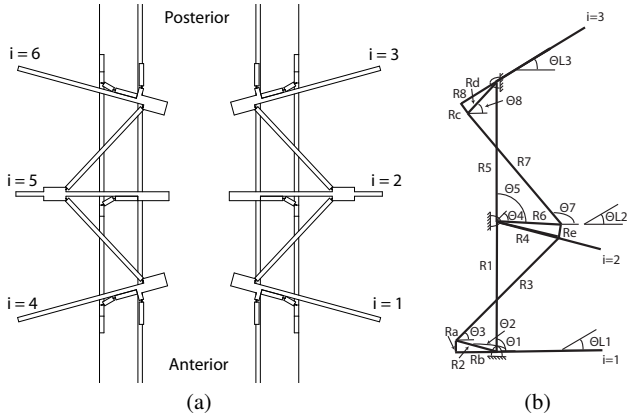

Fig. 3 a) HAMR's thoracic mechanics design with leg numbering convention that is used in this paper. b) Kinematics of HAMR's thoracic mechanics

The kinematic coupling of a single transmission requires that the angles, θ_i of each outer leg $(i = 1,3)$ move in the same direction, while the center leg $(i = 2)$ moves with opposite sign. To determine the orientation, θ_i of each leg coupled by a single transmission, we can analyze the forward kinematic mapping of the two four-bar mechanisms that comprise each transmission given a single input angle the most anterior leg θ_{L1}. Analysis of the linkages labeled in Fig. 3 was done assuming

each link is rigid and each joint is a pin joint. Using four-bar mechanism kinematic analysis software from [20], the lower four-bar mapping (θ_{L2} output) is

$$\theta_{L2} = \theta_4 = atan2(y_1, x_1) - cos^{-1}((x_1^2 + y_1^2 + R_4^2 - R_3^2)/(2R_4\sqrt{x_1^2 + y_1^2})) \quad (1)$$

where $x_1 = R_1 \times \cos(\theta_1) - R_2 \times \cos(\theta_2)$, $y_1 = R_1 \times \sin(\theta_1) - R_2 \times \sin(\theta_2)$, R_{1-4} are known link lengths, and θ_1 is the known ground link orientation. We can again use eqn.(1) to calculate θ_{L3} using θ_{L2} as input. This yields

$$\theta_{L3} = atan2(y_2, x_2) - cos^{-1}((x_2^2 + y_2^2 + R_8^2 - R_7^2)/(2R_8\sqrt{x^2 + y^2})) - \tan^{-1}(R_c/R_d) \quad (2)$$

Where $x_2 = R_5 \times \cos(\theta_5) - R_2 \times \cos(\theta_6)$, $y_2 = R_5 \times \sin(\theta_5) - R_6 \times \sin(\theta_6)$, $R_{5,7,8}$ and θ_5 are known, $R_6 = \sqrt{R_4^2 - R_e^2}$, $\theta_6 = \theta_4 + asin(R_e/R_4)$. Eqns.(1), (2) map input angle to output angles for one half of a leg-stroke. The thoracic mechanics are driven by two sets of proximal actuators (driving θ_{L1}). The stance is determined by distal knee actuators described in sec. 2.2.1.

2.1.2 Proximal Actuation

Shape memory alloy (SMA) and piezoelectric actuators were considered for proximal actuation. Piezoelectric actuators provide benefits such as greater efficiency and bandwidth, and will be considered for future iterations to achieve dynamic gaits. However, for this version of HAMR we chose SMA for ease of powering, control, and integrability. SMA materials can be actuated simply by Joule heating and therefore require only a switched current source as detailed in sec. 2.3. SMA actuators, as opposed to piezoelectric cantilever or stack actuators, require minimal additional transmission to convert small oscillatory motions into the desired leg swing.

Discrete SMA actuators are unidirectional linear actuators, and therefore a single DOF requires an antagonist pair (Fig. 4). Each of HAMR's four thorax actuators control a unipolar motion of one leg transmission. A two-dimensional spring design (Fig. 5) was chosen since it provides linear actuation when pre-strained in tension, and receives a larger displacement in a smaller actuator length than a wire. Since we are using a linear actuator to move along a radial path, HAMR's proximal actuators are oriented parallel to the sagittal plane to prevent singularities. A flexible attachment is provided to prevent the actuator from bending across its thickness, and is therefore constrained to motion in a single plane. To characterize our spring design, we tested output displacement for a single SMA spring acting against an antagonist. The resulting displacement was approximately 300 μm.

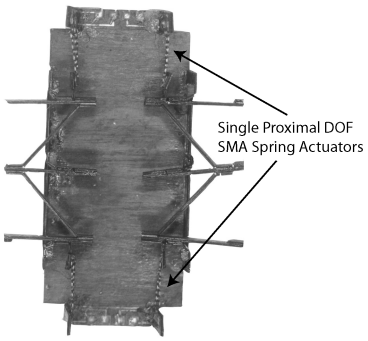

Fig. 4 HAMR's thorax and leg transmission. Each transmission DOF requires two SMA spring actuators. A flexure joint between actuator and transmission prevents singularities and restricts actuator movement to a single plane.

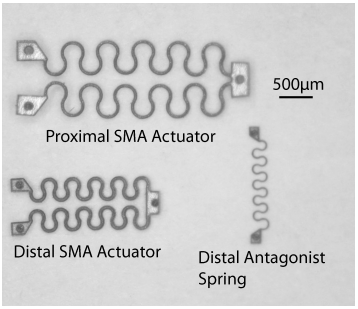

Fig. 5 HAMR's Proximal and distal actuators.

2.2 Leg Mechanics

HAMR's legs, each of which has an articulated knee joint, allows addition or subtraction of a leg from the stance set. Including thorax and legs, there are a total 8 DOFs, each driven with binary actuation and therefore we may define 2^8 or 256 stances. Many of these stance patterns are useless to locomotion, but by transitioning between various stances we may prescribe numerous gaits including alternating tripod, zero-radius turns, and pre-loading attachment mechanisms for wall climbing.

2.2.1 Distal Actuation

HAMR's distal motion is provided by SMA actuators, however they function as cantilevers rather than the planar spring in Section 2.1.2. To conserve power during immobile stance phases, HAMR's knee joints are held down with a passive antagonist 2D spring (Fig. 5) and actuated to a raised position. Because of the simplicity

and short time constant of thin foil spring fabrication (See Section 3.2), we used an iterative design process to find an appropriate force/displacement balance for leg actuation. This balance included a large displacement with a short full-cycle actuation time. Fig. 6 shows the maximum attainable actuated displacement of our design of 9.1 degrees.

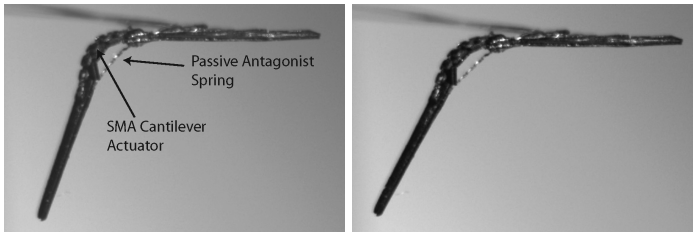

(a) (b)

Fig. 6 HAMR's leg a) unactuated and b) actuated to maximum displacement. The maximum measured angle was 9.1 degrees.

To further inform our design we determined optimal actuation parameters. First, we experimentally determined the current limits for each actuator, the lower limit being necessary for Martensite-Austenite transition and upper limit causing the bonding solder to melt. These limits are 100-150mA and 200-300mA for proximal and distal actuators, respectively. Using ProAnalyst 2D motion tracking software, we characterized the optimal current amplitude and pulse width for distal actuation. Here, optimal is defined as minimum overall actuation period (upstroke and downstroke) while maintaining at least 90 percent of maximum displacement. However in future iterations with on-board power we will also consider energy efficiency as a metric. For these tests the series resistance (See Fig. 7) was tuned to 5Ω and voltage was varied to obtain a current. The optimal leg actuation parameters are 280mA for 0.24s. This corresponds to 274mW power dissipation across the 3.5Ω SMA, and a total of 66mJ of energy per leg, per cycle.

2.3 Power and Control Electronics

HAMR's power electronics must be capable of driving four proximal SMA actuators each with 5.5Ω resistance and six distal actuators each 3.5Ω . We have experimentally determined that each thorax actuator requires 100-150mA and each leg actuator requires 200-300mA for actuation. We simply use ten *n*-type metal oxide semiconductor (NMOS) switches for binary control of the actuators with current tuned by 10Ω potentiometers in series with each actuator. The input signals are generated using Simulink and an xPc target system, which mimics the functionality of an in-

tegrated microcontroller, a feature of future iterations. Fig. 7 shows a schematic of the drive circuitry.

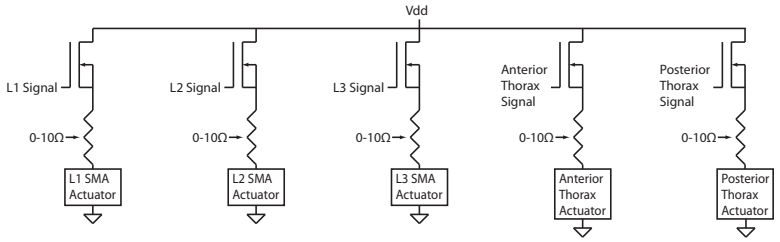

Fig. 7 Circuit drive for one of two contralateral actuator sets.

3 Fabrication Processes

When considering available fabrication techniques, millimeter-scale structures lie in an unconventional size regime. The overall system is too large to use micro-electromechanical system (MEMS) fabrication exclusively, however too small for macro-scale machining. Additionally, when creating articulated structures at the millimeter-scale we are unable to consider classic revolute and telescopic joints or motors since they become inefficient as surface area effects become more relevant than Newtonian forces [23]. Therefore HAMR's physical structure was created utilizing the smart composite microstructure (SCM) manufacturing paradigm [25].

3.1 Smart Composite Microstructures

SCM fabrication utilizes laser-micromachining to pattern two structural composites and a flexible polymer layer, which assemble to form complex 3D articulated microstructures. Using the fabrication process detailed in Fig. 8, we created three leg transmission components (Fig. 9) from M60J carbon fiber laminates and 7.5μm polymide film that assemble into a complete eight DOF mechanism. Articulation is afforded through flexure joints, which exist where cuts in the composite face sheets allow the polymer to bend. This technique of creating flexures also enables the creation of sacrificial flexure joints, thereby creating 3D structures.

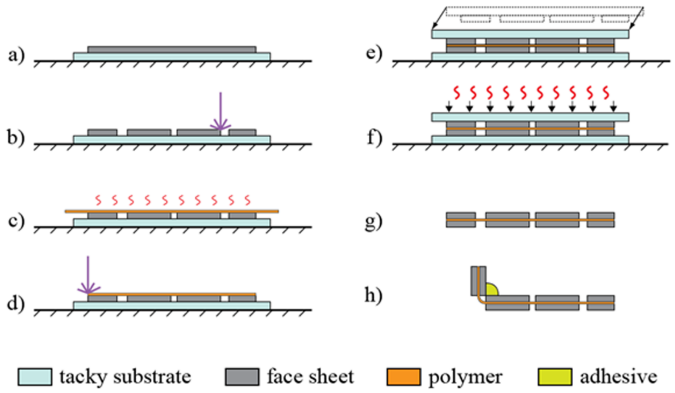

Fig. 8 SCM Fabrication process flow for creating flexure-based articulated structures. Carbon fiber prepreg (a) is laser micromachined to create a face sheet (b) and a polymer layer is debulked onto the face sheet (c). The polymer is patterned using different laser settings (d) and aligned to a second face sheet using kinematic mounts or optical alignment techniques (e). This laminate is vacuum bagged and cured (f). The quasi-planar stucture is released (g) and subsequently folded into 3D shapes (h).

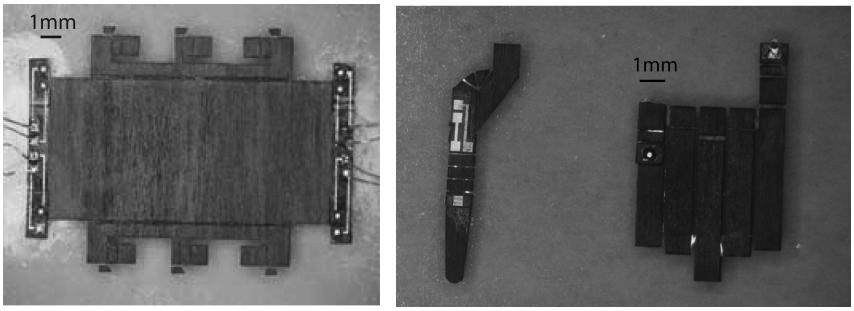

(a) (b)

Fig. 9 HAMR's leg and transmission parts before folding to a 3D structure: a) Thorax b) Leg and leg transmission.

3.2 Actuators, Attachment Mechanisms, and Electronics

3.2.1 Actuators

HAMR's two dimensional shape memory alloy (SMA) actuators were laser-cut from 50μm Nitinol sheets. As detailed in Sec. 2.2.1, passive springs were used as an antagonist for leg actuation. These springs were laser-cut from 25μm stainless steel. Similarly, ribbed attachment mechanisms for rough vertical terrain were cut

from 50μm stainless steel. Fabrication of all three thin-foil metal structures required approximately one minute per batch.

3.2.2 Flexible Circuits

Flexible circuits are used to create an electrical path between HAMR's power input lines and each actuator. Using conventional photolithographic methods, circuits are fabricated from a 12.5 μm copper layer deposited on a 12.5 μm flexible polyimide layer. The resulting compliant circuits (Fig. 10a) are layered on the microstructures and cured along with the entire laminate. The entire structure may be fold-assembled without fracturing the copper traces. Using this process we created 500μm square solder terminals connected by 125μm thick wire traces. Future iterations will use flex circuits to house on-board power and control electronics. We also implemented flex circuits to increase joint rigidity by soldering across two terminals placed on orthogonal surfaces (Fig. 10b).

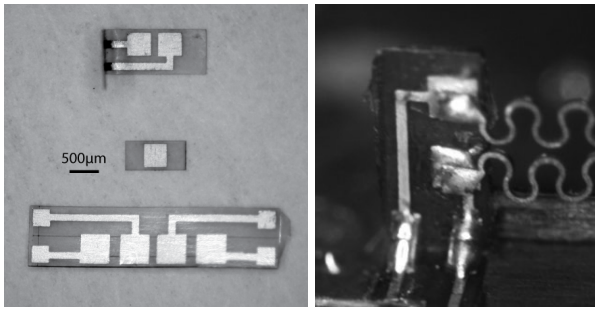

(a) (b)

Fig. 10 a) Flex circuits trace power to HAMR's actuators. The copper traces may be folded without fracturing (top circuit). b) Solder is used structurally to increase joint strength once folded into the desired configuration.

4 Results

HAMR is capable of displaying various leg gaits such as an alternating tripod and static zero-radius turns. To demonstrate gaits we actuated using our empirically-derived optimal parameters, defined here as minimizing simulated actuation period while obtaining maximum leg deflection. Using ProAnalyst 2D motion tracking software to plot leg deflection for various energy inputs, we determined the maximum actuated leg angle to be 9.1 degrees. The parameters to obtain maximum angle at minimum speed are 280mA with a 0.24s pulse width. In the future we must con-

sider energy usage in our description of optimality to conserve the limited lifetime of on-board power.

4.1 Alternating Tripod Gait

We were able to display the most fundamental gait to hexapod locomotion, the alternating tripod at 1/3Hz and 1Hz (See Fig. 11).

We were able to increase actuation speed up to 1 Hz, however this decreased leg displacements. Using ProAnalyst motion capture software we were able to track joint angles during a 1Hz alternating tripod gait. Fig. 13 plots transmission and leg joint angles over three periods, and tab. 1 gives the total measured sweep angle of each joint. By inspection, the 1Hz actuation cycle produces smaller proximal actuation displacements.

Table 1 Total measured sweep angle of each joint at 1Hz operation. All angles measured in degrees

Leg	1	2	3	4	5	6
Maximum Transverse Angle	2.4187	2.5458	3.2078	2.9191	3.8016	3.1618
Maximum Leg Angle	6.3407	5.1809	8.4887	8.4985	5.9961	5.8315

We were also able to demonstrate locomotion on a flat surface using the alternating tripod gait (Fig. 12) at approximately 1cm/min.

4.2 Turning

With a similar actuation scheme to alternating tripod, we are able to demonstrate the mechanics for a zero-radius turn. By maintaining identical tripod stance and swing groupings but actuating the transmissions in phase we obtain these mechanics. This turn requires one or more stance legs to slip. An alternative static turn mechanism is to pivot the body about one fixed ground leg, which is also achievable.

4.3 Attachment

This paper covers the numerous difficulties faced when designing a robotic insect, however it is important to note the benefits of small-scale robots with regards to wall attachment. Insects are capable of adhering to many vertical and inverted surfaces with attachment mechanisms such as tarsal claws [18], capillary adhesion [7] and Van Der Waals adhesion [2]. An un-actuated clawed version of HAMR illustrates the possibility of rough vertical surface attachment (Fig. 14a). Each leg includes

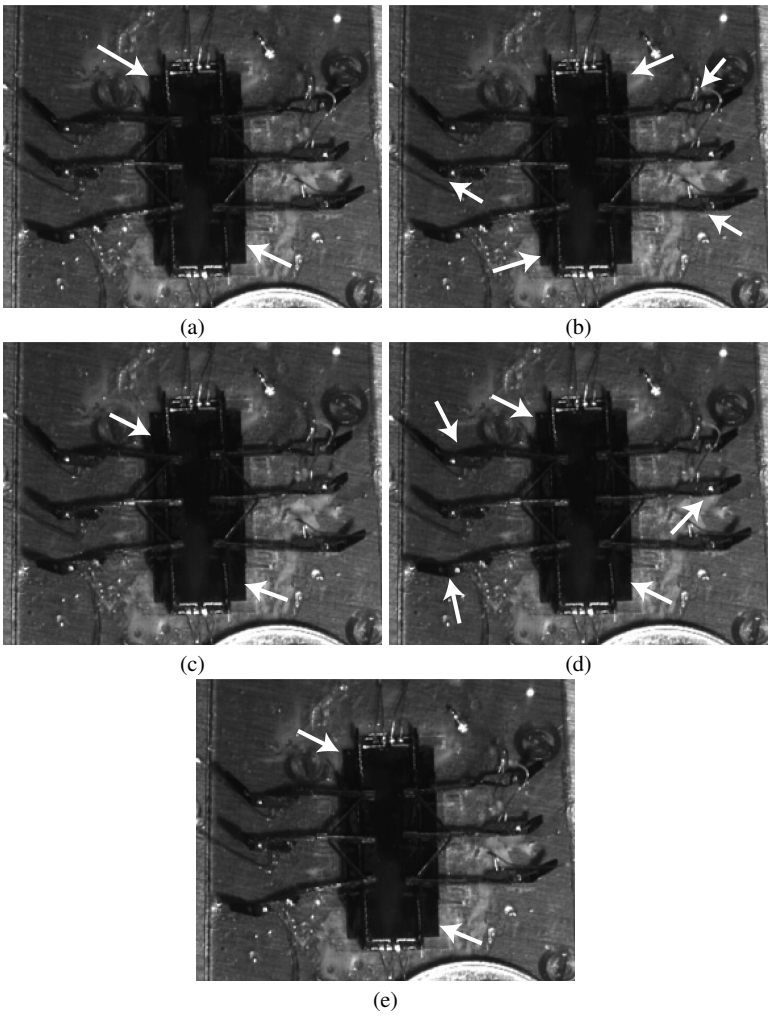

Fig. 11 The alternating tripod gait at 1/3Hz while suspended. Anterior is towards the bottom of the image, and arrows indicate powered actuators. a) All six legs are in stance while leg groupings change. b) Legs 1,3,5 are in swing. c) All six are again ground during a transition. d) Legs 2,4,6 are in swing. e) All six are again in stance at the end of the period.

an attachment mechanism containing eleven 200μm claws (Fig. 14b). They allow HAMR to support greater than 100 times its body weight while hanging from three legs on a rough felt surface (Fig. 14c). This experiment does not prove vertical locomotion but provides the foundation of research on one form of dry adhesion. Further research will explore the claw geometry [1] and body mechanics necessary to climb vertical surfaces of varying roughness.

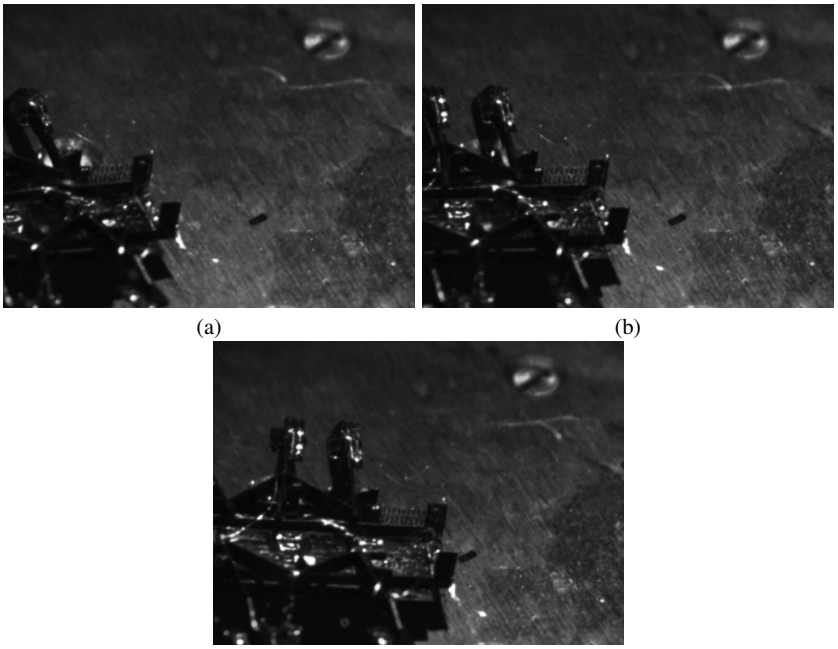

(a) (b)

(c)

Fig. 12 Locomotion on a flat surface at 1/3Hz using the alternating tripod gait. a) at 0 seconds, b) at 15 seconds, c) at 30 seconds.

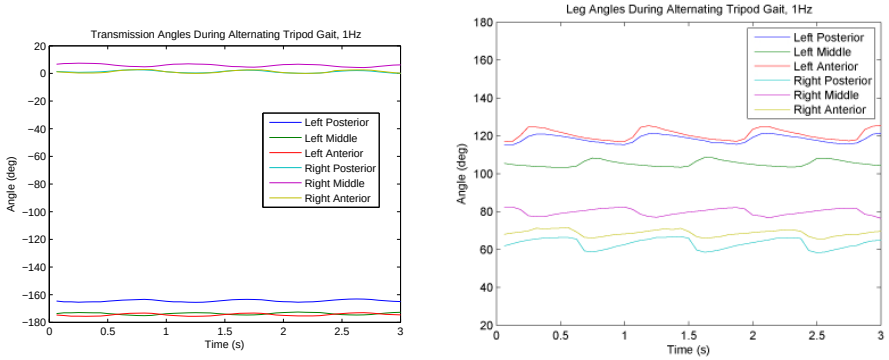

(a) (b)

Fig. 13 a) Motion capture software is used to track HAMR's a) transmission angles and b) leg angles over three periods of 1Hz motion.

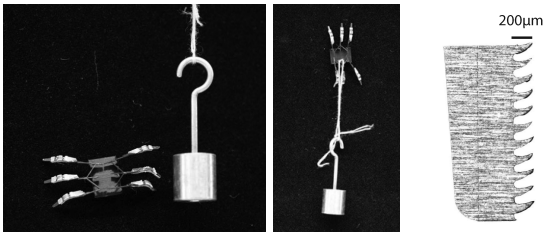

(a) (b) (c)

Fig. 14 100 mg, unactuated, clawed version of HAMR. Outfitting the legs with attachment claws facilitates hanging a) in the direction of a vertical climb, b) while supporting a 10 g weight. c) Close-up of HAMR's 200μm claws.

5 Conclusions / Future Work

This paper has proven the feasibility of creating a hexapedal ambulatory microrobot with dynamic gait modulation. We have demonstrated the alternating tripod gait and zero-radius turns at 1/3Hz and 1Hz, and a simple mechanism for attachment to moderately rough surfaces. There is significant work yet to complete to create an autonomous, untethered, millimeter scale hexapod mobile robot capable of traversing any terrain, however this paper presents the initial steps.

5.1 Actuation and Control

Future work will include a thorough study of thin foil SMA actuators as well as exploration of other actuation alternatives such as piezoelectric ceramics and active fiber composites. As stated in Section 4.1, by increasing actuation speed from 1/3 to 1Hz we reduce thoracic actuator displacement, presumably because at the higher speed we do not allow actuator temperature to reach the required level. Therefore, we require a comprehensive model of thermodynamic and mechanical properties of our SMA spring to inform future designs. We must also model our distal actuators to achieve an appropriate force/displacement balance to clear a reasonable height during swing phases, yet produce enough force to overcome friction when lifting off the walking terrain.

As previously stated, HAMR will be untethered in future iterations by integrating an on-board power supply and microcontroller. Not only is this important for autonomy, but it is imperative to achieve forward locomotion since the tethering wires greatly outweigh the thorax and leg masses. Integrated power and control will also allow us to modulate the current to each of the 10 actuators, giving us more control over actuation timing. An onboard controller will also allow us to actuate with non-constant current. Actuator efficiency will increase with more complex control signals such as a short spike to quickly heat the SMA, followed by a lower, constant

current to keep the actuator above its transition temperature [10]. This will have several effects such as reducing the thermal time constant of cooldown and prolonging the actuator lifetime.

5.2 Vertical Locomotion

Further research will explore the mechanics of wall-climbing, including attachment mechanisms for rough and smooth surfaces, transitions between orthogonal surfaces, and animal climbing mechanics.

6 Acknowledgements

The authors gratefully acknowledge The Charles Stark Draper Laboratory and the National Science Foundation (award number 0811571) for support of this work. Any opinions, findings, and conclusions or recommendations expressed in this material are those of the authors and do not necessarily reflect the views of the National Science Foundation.

References

1. A.T. Asbeck, S. Kim, MR Cutkosky, W.R. Provancher, and M. Lanzetta. Scaling hard vertical surfaces with compliant microspine arrays. *The International Journal of Robotics Research*, 25(12):1165, 2006.
2. K. Autumn, M. Sitti, Y.A. Liang, A.M. Peattie, W.R. Hansen, S. Sponberg, T.W. Kenny, R. Fearing, J.N. Israelachvili, and R.J. Full. Evidence for van der Waals adhesion in gecko setae. *Proceedings of the National Academy of Sciences*, 99(19):12252–12256, 2002.
3. S. Bergbreiter and K.S.J. Pister. Design of an autonomous jumping microrobot. In *IEEE Int. Conf. on Robotics and Automation*, Roma, Italy, April 2007.
4. N.J. Cowan, E.J. Ma, M. Cutkosky, and R.J. Full. A biologically inspired passive antenna for steering control of a running robot. *Springer Tracts in Advanced Robotics*, 15:541–550, August 2005.
5. B.R. Donald, C.G. Levy, C.D. McGray, and D. Rus. An untethered, electrostatic, globally controllable mems micro-robot. *J. of Microelectrical Mechanical Systems*, 15:1–15, February 2006.
6. T. Ebefors, J.U. Mattsson, E. Kälvesten, and G. Stemme. A walking silicon micro-robot. In *The 10th Int. Conf. on Solid-State Sensors and Actuators (Transducers '99)*, pages 1202–1205, Sendai, Japan, June 1999.
7. J.S. Edwards and M. Tarkanian. The adhesive pads of Heteroptera: a re-examination. In *Proceedings of the Royal Entomological Society of London. Series A, General Entomology*, volume 45, pages 1–5. Blackwell Publishing Ltd, 1970.
8. R.J. Full and M.S. Tu. Mechanics of a rapid running insect: two-, four- and six-legged locomotion. *J. of Experimental Biology*, 156:215–231, 1991.
9. D.I. Goldman, T.S. Chen, and D.M. Dudek. Dynamics of rapid vertical climbing in cockroaches reveals a template. *Journal of Experimental Biology*, 209(15):2990, 2006.

10. A.M. Hoover, E. Steltz, and R.S. Fearing. Roach: An autonomous 2.4g crawling hexapod robot. In *IEEE/RSJ Int. Conf. on Intelligent Robots and Systems*, Nice, France, September 2008.
11. S. Kim, A.T. Asbeck, M.R. Cutkosky, and W.R. Provancher. Spinybotii: Climbing hard walls with compliant microspines. In *IEEE Int. Conf. on Advanced Robotics*, Seattle, WA, July 2005.
12. S. Kim, M. Spenko, S. Trujillo, D. Santos, and M.R. Cutkosky. Smooth vertical surface climbing with directional adhesion. *IEEE Transactions on Robotics*, 24:65–74, February 2008.
13. J. Lee, S.N. Sponberg, O.Y. Loh, A.G. Lamperson, R.J. Full, and N.J. Cowan. Templates and anchors for antenna-based wall following in cockroaches and robots. *IEEE Transactions on Robotics*, 24(1), February 2008.
14. W.A. Lewinger, C.M. Harley, R.E. Ritzman, M.S. Branicky, and R.D. Quinn. Insect-like antennal sensing for climbing and tunneling behavior in a biologically-inspired mobile robot. In *IEEE Int. Conf. on Robotics and Automation*, Seattle, WA, July 2005.
15. J.M. Morrey, B. Lambrecht, A.D. Horchler, R.E. Ritzmann, and R.D. Quinn. Highly mobile and robust small quadruped robots. In *IEEE/RSJ Int. Conf. on Intelligent Robots and Systems*, Las Vegas, NV, October 2003.
16. M. Raibert, K. Blankespoor, G. Nelson, and R. Playter. Bigdog, the rough-terrain quadruped robot. In *Proc. of the 17th World Congress*, Seoul, Korea, July 2008.
17. L.M. Roth and E.R. Willis. Tarsal structure and climbing ability of cockroaches. *J. of Exp. Zool.*, 119(3):483–517, April 1952.
18. L.M. Roth and E.R. Willis. Tarsal structure and climbing ability of cockroaches. *Journal of Experimental Zoology*, 119(3), 1952.
19. U. Saranli, M. Buehler, and D.E. Koditschek. RHex - a simple and highly mobile hexapod robot. *Int. J. of Robotics Research*, 20:616–631, July 2001.
20. SoftIntegration. Interactive four-bar linkage position analysis.
21. S. Sponberg and R.J. Full. Neuromechanical response of musculo-skeletal structures in cockroaches during rapid running on rough terrain. *J. of Experimental Biology*, 211:433–446, May 2008.
22. D. Teasdale, V. Milanovic, P. Chang, and K.S.J. Pister. Microrockets for smart dust. *Smart Materials and Structures*, 6:1145–1155, November 2001.
23. W.S.N. Trimmer. Microrobots and micromechanical systems. *J. of Sensors and Actuators*, 19:267–287, 1989.
24. R.J. Wood. The first flight of a biologically-inspired at-scale robotic insect. *IEEE Transactions on Robotics*, 24(2), April 2008.
25. R.J. Wood, S. Avadhanula, R. Sahai, E. Steltz, and R.S. Fearing. Microrobot design using fiber reinforced composites. *J. of Mech. Design*, 130(5), May 2008.
26. R.J. Wood, S. Avadhanula, E. Steltz, M. Seeman, J. Entwistle, A. Bacharach, G. Barrows, S. Sanders, and R.S. Fearing. Design, fabrication and initial results of a 2g autonomous glider. In *Conf. on IEEE Industrial Electronics*, Raleigh, NC, November 2005.
27. R. Yeh, S. Hollar, and K.S.J. Pister. Design of low-power silicon articulated microrobots. *J. of Micromechatronics*, 1(3):191–203, 2002.